



TECHNICAL ARTICLE

# Hot Gas Pressure Forming and Post Aging Treatment of Ti-22Al-24.5Nb-0.5Mo Square Tubes

Zhiqiang Liu, Xueyan Jiao, Dongjun Wang, Shiqiang Zhu, Dagang Wang, and Gang Liu

Submitted: 2 September 2021 / Revised: 9 November 2021 / Accepted: 28 November 2021 / Published online: 30 January 2022

The forming of Ti-22Al-24.5Nb-0.5Mo alloy tubular component with square cross section was studied by simulation and experiment. The wall thickness distribution, radius of the fillet, microstructure and mechanical properties of formed tubes were investigated in the paper. Results demonstrated that the time required for the corner forming was gradually reduced with the increasing forming temperature. When the forming temperature was above 970 °C, the formed parts were good in thickness uniformity with maximum thinning ratio less than 19%. The lamellar O phase dissolved in forming process and precipitated during the aging process. The tensile strength at 750 °C increased with forming temperature. The elongation-to-failure at 750 °C decreased with the increase in strength. After post aging treatment, the elongation-to-failure at 750 °C was significantly improved. The strength of 788 MPa and elongation-to-failure of 11.1 % were achieved when the tube formed 970 °C and post aged at 800 °C. The geometrical shape and microstructure of the formed square tubes were simulated accurately by the uniform viscoplastic constitutive model of Ti<sub>2</sub>AlNb alloy.

**Keywords** aging treatment, hot gas pressure forming, simulation, square cross-section tube, Ti<sub>2</sub>AlNb-based alloy

## 1. Introduction

With the development of aviation and aerospace industry, heat-resistant and lightweight components are in urgent need to improve the performance of aircraft engine (Ref 1, 2). The Ti<sub>2</sub>AlNb-based alloys have far reaching application potential in the aviation and aerospace industry because of its sufficient creep resistance, high specific strength and good oxidation resistance at elevated temperatures (Ref 3-6). The alloy can be used at 650-750 °C for a long time (Ref 7). Therefore, the forming of hollow thin-walled components made of Ti<sub>2</sub>AlNb-based alloys has become one of the research focuses in the aviation and aerospace industry.

Because of the intrinsic brittleness and high deformation resistance, the forming of Ti<sub>2</sub>AlNb thin-walled components with irregular cross section are very difficult (Ref 8, 9). Only a few researches focused on the forming of complex Ti<sub>2</sub>AlNb components has been reported. Generally, the superplastic forming technology has been widely used in the forming of the complex thin-walled

components made of difficult-to-deformation alloys (Ref 10-13). Nevertheless, the application of the forming technology has been limited because of its grueling forming condition (such as high forming temperature, low strain rate and fine grain), low efficiency, high energy consumption and microstructure damage. In this case, hot gas pressure forming technology (HGPF) has been developed on the basis of superplastic forming and received more and more attention. Hot gas pressure forming technology shows obvious advantages such as high forming precision, and efficiency in the forming of hollow thin-walled components. Typically, the hot gas pressure forming was mainly used to the forming of aluminum alloy (Ref 14), magnesium alloy (Ref 15), stainless steel (Ref 16) and titanium alloy (Ref 17, 18). Few researches focused on the forming of high-strength intermetallic, for instance, Ti<sub>2</sub>AlNb alloy. The microstructure of Ti<sub>2</sub>AlNb alloy was sensitive to the forming parameters. And mechanical properties were affected by microstructure. Therefore, it is important to systematically investigate effect of the hot gas pressure forming parameters on the forming property, microstructure and mechanical properties of Ti-22Al-24.5Nb-0.5Mo alloys components with square cross section. The simulations based on the uniform viscoplastic constitutive equations were also conducted in the article. In addition, subsequent heat treatment was necessary to optimize the microstructure and mechanical properties of the formed components to achieve optimized performance. The deformation was conducted in the in temperature range of 950-990 °C. And the post aging temperature was in the range of 750-850 °C. The effect of the process parameters on radius of the fillet, wall thickness distribution, microstructure and mechanical properties was investigated.

## 2. Experimental Material and Procedure

The hot-rolled sheet of Ti-22Al-24.5Nb-0.5Mo (at.%) was used in the experiment. The thickness of sheet was 2.0 mm. Fig. 1(a) displays the microstructure of experimental alloy, the

Zhiqiang Liu, Dongjun Wang, and Gang Liu, National Key Laboratory for Precision Hot Processing of Metals, Harbin Institute of Technology, Harbin 150001, China; and School of Materials Science and Engineering, Harbin Institute of Technology, Harbin 150001, China; Xueyan Jiao, School of Materials Science and Engineering, Harbin Institute of Technology, Harbin 150001, China; and College of Naval architecture and Marine Engineering, Shandong Jiaotong University, 1508 Hexing Road, Weihai 264310, China; Shiqiang Zhu and Dagang Wang, Capital Aerospace Machinery Company, Beijing 100076, China. Contact e-mail: gliu@hit.edu.cn.

microstructure was typical bimodal morphology, comprised of  $\alpha_2$  phase, O phase and the matrix  $\beta$ /B2 phase. The selected forming temperature was 950-990 °C. The temperatures were in B2+O+ $\alpha_2$  phase region according to the equilibrium phase diagram of Ti-22Al-xNb shown in Fig. 2 (Ref 19). The Ti<sub>2</sub>AlNb alloy has good formability and plasticity at 950-990 °C (Ref 20). When the forming temperature was lower than 950 °C, the elongation of the alloy was poor and the strain softening phenomenon was more obvious (Ref 20), which was detrimental to the formability of the alloy and uniformity of wall thickness of formed components. Fig. 1(b), (c) demonstrate the true stress-strain curves of the as-received sheets at 950-990 °C with strain rate of 0.01-0.001 s<sup>-1</sup>. It was observed that the flow stress was effected by the deformation temperature and strain rate sensitively, which increased with the decreasing temperature and increasing strain rate. The strain softening phenomenon occurred obviously in the tensile test at 950 °C, while it became inconspicuous at 970-990 °C. Lowering the strain rate to 0.001 s<sup>-1</sup>, the elongation-to-failure ( $(l_{failure} - l_0)/l_0 \times 100\%$ , where  $l_{failure}$  and  $l_0$  were length of fractured specimen and initial length) could reach 161.4, 245.8 and 179.0% at 950, 970 and 990 °C, respectively.

The tubes with a diameter of 40 mm were used in the experiment, which were fabricated by U-O forming and laser-beam welding, as shown in Fig. 3(a), (b). The experiments were conducted on a self-designed HGPF platform. The platform consisted of temperature control system, pressure loading system, press and dies. It was able to provide loading pressure up to 70MPa, the pressure control accuracy was  $\pm 0.1$ MPa. Induction heating was used in the platform. Maximum forming temperature was 1050 °C, control accuracy was  $\pm 5$  °C. The specific die is shown in Fig. 3(c). Two thermocouples were applied to measure the temperatures of the die and tube, respectively. When the die reached the forming temperature, the tubes were transferred to the die within 20 s. After reaching the forming temperature, the tube was kept for 15min. The instant displacement of the horizontal corner of the tube was measured and recorded by displacement sensor to monitor the deformation state during experiments. After HGPF process, the square tubes were transferred to cold water within 20 s.

The microstructures were observed by scanning electron microscopy (Quanta 200FEG). Vickers hardness was measured by microhardness instrument (FM-700e). The load was 500 g, and dwell time was 10 s. Moreover, the tensile properties at 750 °C for the formed square tubes were tested on an Instron 5500R electronic testing machine with strain rate of  $1 \times 10^{-3}$  s<sup>-1</sup>.

The specimens were cut from the straight region of the square tubes (i.e., SR in Fig. 3d) by WEDM (wire electrical discharge machining). The gauge dimension of the specimen was 15 mm $\times$ 3 mm.

### 3. Results and Discussion

#### 3.1 Simulation

The forming of square tubes with HGPF process was simulated at 950, 970 and 990 °C, respectively. The forming pressure was 15 MPa. The simulations were conducted by the commercial FEM software ABAQUS. A self-designed uniform viscoplastic constitutive model of Ti<sub>2</sub>AlNb alloy based on microstructure internal state variables was embedded in the ABAQUS by the subroutine VUMAT. The constitutive model

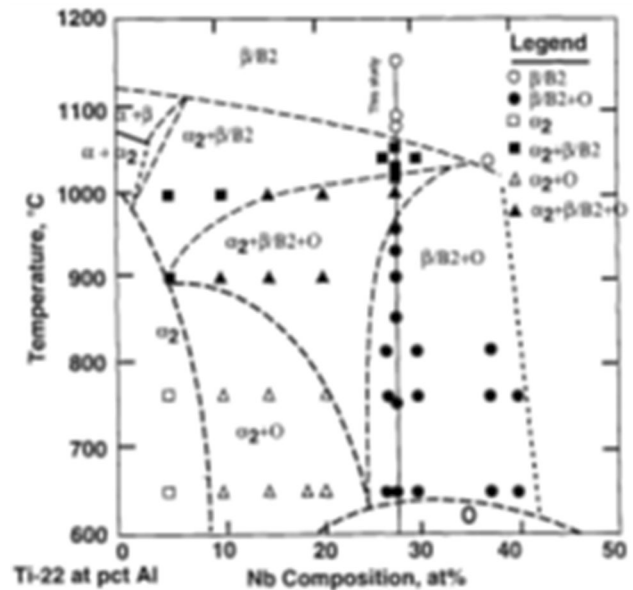


**Fig. 2** Equilibrium phase diagram of Ti-22Al-xNb. Republished with permission of ASM International, from The Phase Evolution and Microstructural Stability of an Orthorhombic Ti-23Al-27Nb Alloy, Zhiqiang Liu, Xueyan Jiao, Dongjun Wang, Shiqiang Zhu, Dagang Wang, Gang Liu, *Journal of Phase Equilibria and Diffusion*, Volume 20, 1991; permission conveyed through Copyright Clearance Center, Inc. [19]

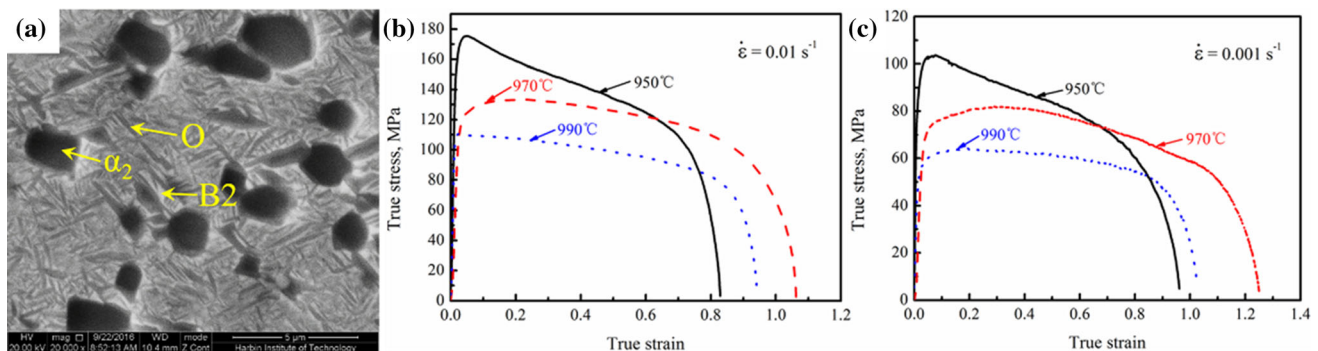


**Fig. 1** Microstructure and stress-strain curves of the experimental Ti-22Al-24.5Nb-0.5Mo alloy at 950-990 °C, (a) SEM microstructure, (b) stress-strain curves with strain rate of 0.01 s<sup>-1</sup>, (c) stress-strain curves with strain rate of 0.001 s<sup>-1</sup>

considered the microstructure evolutions (such as dislocation evolution, damage, dynamic recrystallization, dynamic recovery, spheroidization and grain size evolution) and the relationship between microstructure and mechanical properties during the high-temperature deformation. The constitutive model is shown in Eq 1. Detailed modeling process and model parameters were shown in the article (Ref 20). The model considered the microstructure evolution and deformation history, so the FEM simulation based on the model can predict not only geometrical shape more accurately but also microstructure evolution.

$$\left\{ \begin{array}{l} \dot{\varepsilon}_{p,O} = \left( \frac{\sigma/(1-D) - H - \sigma_{0,O}}{\lambda_{KB2/\beta}(1 - \zeta f_O \omega)} \right)^n (\bar{d})^{-\mu} \\ \dot{\varepsilon}_{p,B2/\beta} = \left( \frac{\sigma/(1-D) - H - \sigma_{0,B2/\beta}}{\lambda_{KB2/\beta}(1 - \zeta f_O \omega)} \right)^n (\bar{d})^{-\mu} \\ H = B\bar{\rho}^{0.5} \\ f_{B2/\beta} = 1 - \psi_1 \exp(\psi_2(T_{T,B2/\beta} - T)) \\ f_O = \psi_3 \exp(\psi_4(T_{T,O} - T)) \\ f_{\alpha_2} = 1 - f_O - F_{B2/\beta} \\ \dot{\varepsilon}_p = f_{B2/\beta} \dot{\varepsilon}_{B2/\beta} + f_O \dot{\varepsilon}_O \\ \dot{S} = \frac{q_1 [x\bar{p} - \bar{\rho}_c(1 - S)](1 - S)^{q_2} \dot{\varepsilon}_p^{q_3}}{\bar{d}} \\ \bar{\rho}_c = q_4 \dot{\varepsilon}_p^{q_5} \\ \dot{x} = q_6(1 - x)\bar{\rho} \\ \dot{\bar{\rho}} = A \dot{\varepsilon}_p^\delta \cdot |\dot{\varepsilon}_p| - k_1 \bar{\rho} \dot{\varepsilon}_p^{\delta_1} \cdot k_2 \bar{\rho} \dot{\varepsilon}_p^{\delta_2} - [k_3 \bar{\rho} / (1 - S)] \dot{S} \\ \dot{\bar{d}} = \alpha_1 \bar{d}^{-\gamma_1} + \alpha_2 \dot{\varepsilon}_p \bar{d}^{-\gamma_2} - \alpha_3 \dot{S}^{\gamma_3} \bar{d}^{\gamma_4} \\ \dot{\omega} = \chi_1(1 - \omega) + (1 - \omega)\chi_2 \dot{\varepsilon}_p^{\chi_3} \\ \dot{T} = \frac{\eta \sigma}{C_v \bar{d}} |\dot{\varepsilon}_p| - \lambda' \Delta T \\ \dot{D} = \eta_1(1 - D) \dot{\varepsilon}_p^{\eta_1} + \eta_2 \dot{\varepsilon}_p^{\eta_2} \exp(\eta_3 \varepsilon_p) - \eta_4 D \\ \sigma = E(1 - D)(1 - \zeta f_O \omega)(\varepsilon^T - \varepsilon^p) \end{array} \right. \quad (\text{Eq 1})$$

Where  $\sigma$  and  $\sigma_0$  were flow stress and initial threshold stress, respectively.  $\varepsilon_p$  was the plastic strain.  $T_{T,B2/\beta}$  and  $T_{T,O}$  were the transformation temperature of  $\alpha_2 \rightarrow B2/\beta$  and  $O \rightarrow B2/\beta$ , respectively.  $f_{B2/\beta}$ ,  $f_O$  and  $f_{\alpha_2}$  were phase content of  $B2/\beta$ ,  $O$  and  $\alpha_2$ , respectively.  $S$  was percentage of dynamic recrystallization.  $T$  and  $\Delta T$  were deformation temperature and temperature rise due to plastic deformation, respectively.  $D$  was the material damage.  $\omega$  was percentage of globularization of lamellar O-grain.  $\bar{d}$  and  $d_0$  were relative grain size and initial grain size, respectively.  $\bar{\rho}$  was the relative dislocation density.  $H$  was the isotropic work hardening. Other parameters appeared in the equations were materials constants.

Figure 4 shows the distribution of thinning ratio ( $(t_0 - t)/t_0 \times 100\%$ , where  $t_0$  and  $t$  were wall thickness of the blanks and the formed parts) of the square tube forming at 990 °C. In the square cross-section region, the maximum thinning ratio was in the transition region (TR region, as shown in Fig. 3(d)) between straight wall region and fillet as shown in Fig. 4(b). The maximum thinning ratio in the square cross-section region were 25.5, 21.3 and 19.9%, respectively, at 950, 970 and 990 °C. Increasing forming temperature would improve the uniformity of the wall thickness at 950-990 °C. The microstructure variables were also been simulated, the phase contents of B2 phase of the formed tubes are shown in

Fig. 5 at 950-990 °C. As shown in the figure, there was little difference in different region of formed tube. The forming temperature was an important factor to affect the phase content. The simulated phase contents of B2 were about 72, 85 and 93%, respectively, at 950, 970 and 990 °C.

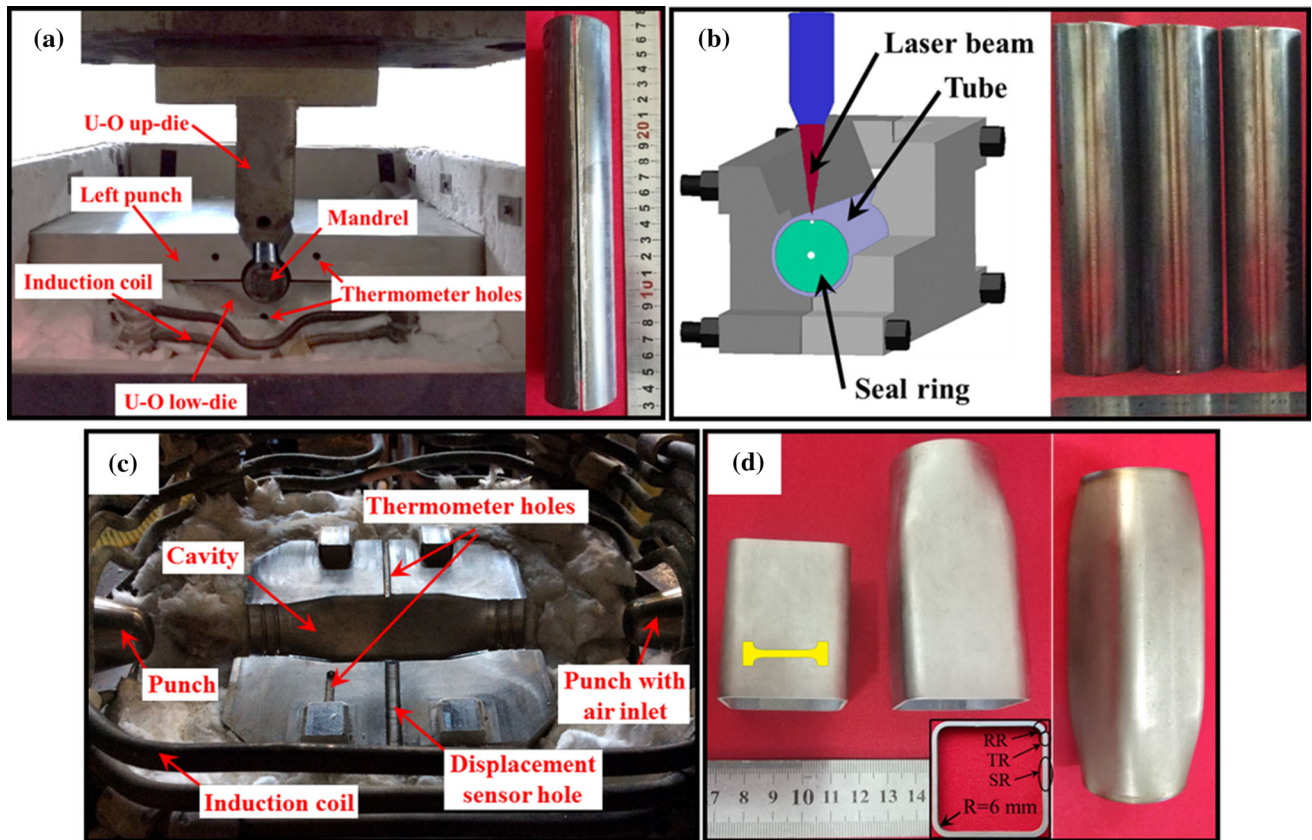
### 3.2 Hot Gas Pressure Forming

The HGPF process was conducted at 950, 970 and 990 °C, respectively, with 15 MPa. The recorded displacement data were used to calculate the instant radius of the fillet. The changes of radius of the fillet with time are shown in Fig. 6(a). According to the pressure loading process, the deformation could be divided into two stages. In the pressure-increasing stage, the tube kept undeformed until it reached the yield condition and then the deformation rate increased with the pressure increasing, resulting in that the forming rate of fillet increased with the pressure increasing. After the pressure-increasing stage, the forming pressure was kept at the constant value, defined as pressure-keeping stage. As the radius of the fillet was further reduced, the stress required to maintain the current deformation rate was increased. The constant forming pressure was insufficient to provide the corresponding stress. Thus, the forming rate of fillet gradually decreased with the decreasing of radius of the until the corner formation finishing. It was observed that the forming rate of fillet increased rapidly at first and then continuously declined until radius of the fillet reached the final dimension of 6 mm. In addition, the time required for the corner forming was gradually reduced with the increasing forming temperature. When the forming temperature increased from 950 to 990 °C, the required forming time reduced from 650 to 220 s accordingly. Fig. 6(b) presents the thickness thinning ratio on the cross section for the square tubes formed at 950, 970 and 990 °C, respectively. As shown in Fig. 6, the maximum thickness thinning took place in the TR region (as shown in Fig. 2d), which was the transition region of straight wall (SR region, as shown in Fig. 2d) and fillet (RR region, as shown in Fig. 2d), because the region could satisfy yielding condition more easily due to the friction on the straight region (Ref 21). Compared with the thickness thinning ratios of the square tubes formed at different forming condition, it indicated that decreasing the forming temperature to 950 °C would increase the wall thickness non-uniformity, which was caused by the significant strain softening (shown in Fig. 1b-c). Furthermore, when the parts were formed at 970 °C and 990 °C, a relative uniform wall thickness distribution could be obtained. The maximum thinning ratio was less than 19%.

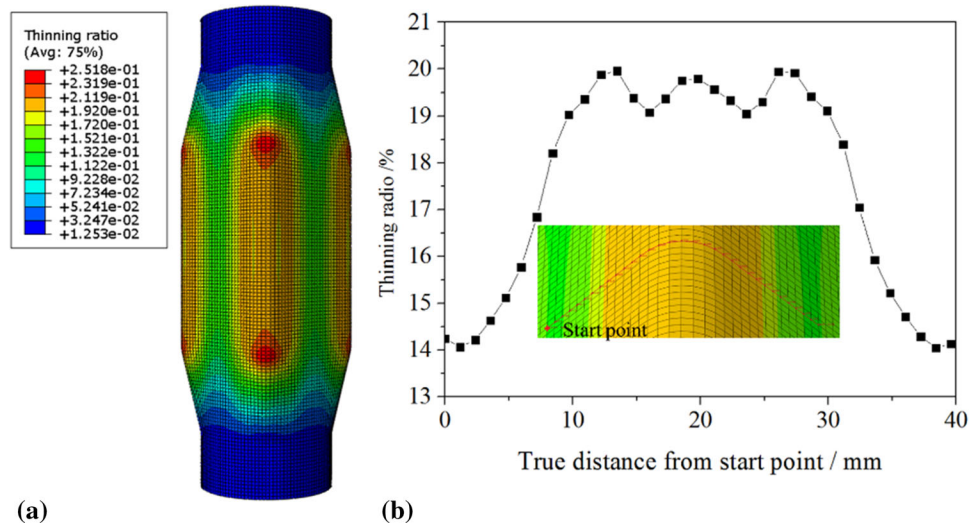
### 3.3 Microstructure Evolution

Figure 7 shows the microstructure of the tubes formed at different temperatures. The forming temperatures were in  $B2+O+\alpha_2$  phase region. The  $O$  phase would dissolve at the temperature. As shown in Fig. 7, grain coarsening of the residual lamellar  $O$  phase took place when the tubes formed at 950 °C. When the forming temperature above 970 °C, most of  $O$  phase would dissolve and almost disappeared in the microstructure. In general, the volume fraction and morphology of phase are one of the most important factor affecting the mechanical properties of the formed tubes (Ref 22, 23). Table 1 displays the corresponding volume fraction of phases. In accordance with the simulation results, the volume fraction of  $\beta/B2$  phase of formed square tubes increased with forming temperature, which was more than the initial tube. Besides,





**Fig. 3** Fabrication of Ti-22Al-24.5Nb-0.5Mo square tubes, (a) U-O forming, (b) laser-welding, (c) hot gas forming, (d) samples of formed square tubes



**Fig. 4** Simulated distribution of thickness thinning ratio of (a) the whole square tube and (b) the square cross section of tube formed at 990 °C

because of the partial dissolution of  $\alpha_2$  phase, the  $\beta/B2$  grains slightly coarsened at 990 °C due to weakening of its pinning effect on  $\beta/B2$  grain boundaries.

The microstructure obtained in the forming temperature had high strength and poor plasticity due to the presence of large amounts of B2 phase. Therefore, in order to control the mechanical properties of parts, aging treatment was carried out to achieve higher plasticity while maintaining strength. Aging

treatment was carried out after gas forming at 970 °C to improve the comprehensive mechanical properties. The samples were aged at 750-850 °C (B2+O phase region, as shown in Fig. 2), respectively, for 10 hours to promote the precipitation of fine O phase, followed by air cooling. Based on the aging microstructures in Fig. 8, one can see that the lamellar O phase re-precipitated from the  $\beta/B2$  phase during the aging treatment. Moreover, the volume fraction and the average width of the

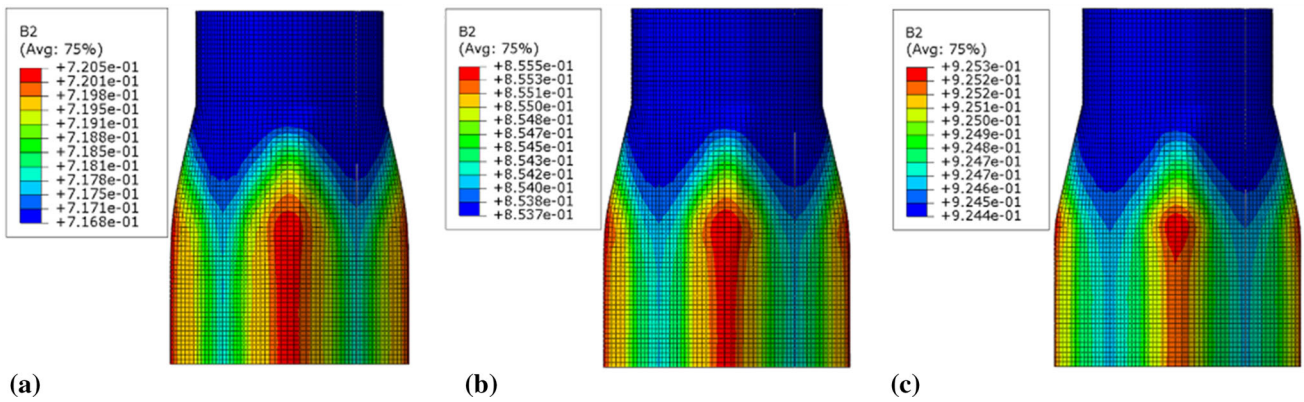


Fig. 5 Phase content of B2 phase of the square tubes formed at (a) 950 °C, (b) 970 °C, (c) 990 °C by simulation

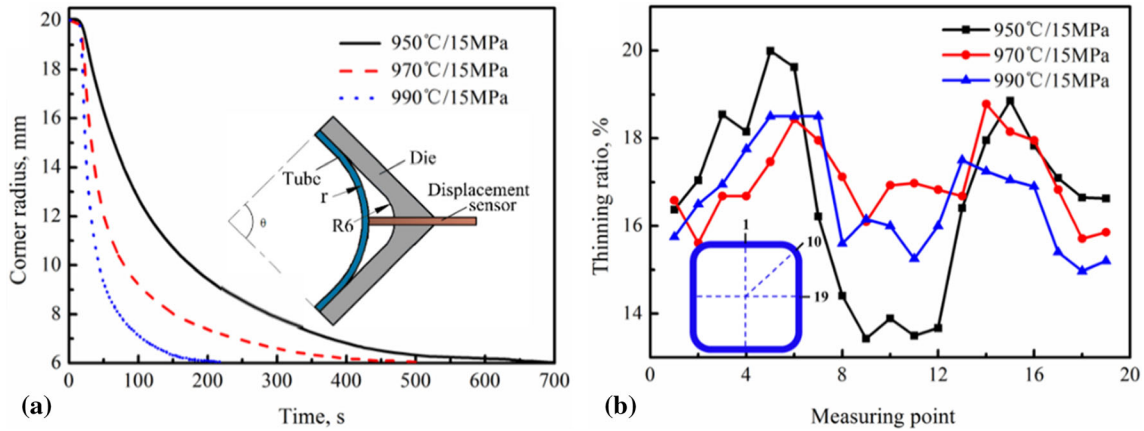


Fig. 6 (a) the corner radius curves during HGPF, (b) distribution of thickness thinning ratio for the square tubes

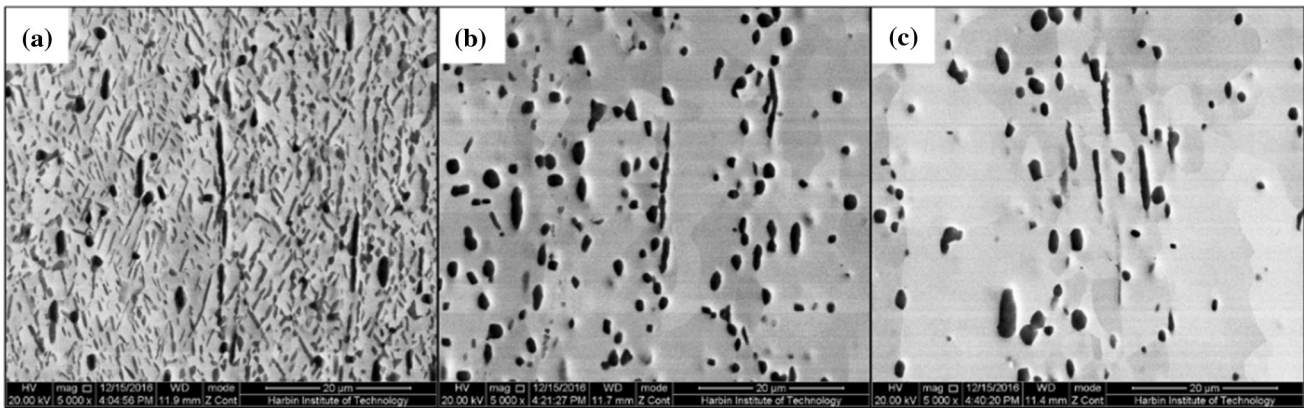


Fig. 7 Microstructure (SR) of the square tubes formed at different temperatures, (a) 950 °C, (b) 970 °C, (c) 990 °C

Table 1 Volume fraction of phases in square tubes fabricated at different temperatures

Forming temperature	950 °C	970 °C	990 °C
Volume fraction of O phase	19.3%	0	0
Volume fraction of $\alpha_2$ phase	8.1%	11.6%	9.3%
Volume fraction of $\beta$ /B2 phase	72.6%	88.4%	90.7%

lamellar O phase increased with the increase in aging temperature, e.g., as the aging temperature increased from 750 to 850 °C, the lamellar O phase width increased from 90 to 200 nm and the volume fraction increased from 42.8 to 45.7% as shown in Table 2.

Figure 9(a) presents the Vickers microhardness of formed tubes. The microhardness slightly decreased with the increase in forming temperature, such as HV 313 at 950 °C and HV 306 at 990 °C. This result was caused by the reduced volume fraction of relatively stronger O and  $\alpha_2$  phases. Figure 9(b) shows the tensile stress-strain curves at 750 °C. The peak stress



of formed tubes increased with the increase in forming temperature at 950-990 °C. The peak stress increased from 793 MPa formed at 950 °C to 920MPa at 990 °C. Meanwhile, elongation-to-failure decreased with the increasing forming temperature. It is worthy to note that the disordered  $\beta$  phase will transform to the ordered B2 phase during the tensile test at 750 °C (Ref 24). Furthermore, compared with the ordered  $\alpha_2$  phase and O phase, the ordered B2 phase is stronger and brittle (Ref 25, 26). Because of the massive formation of ordered B2 phase during the tensile test, the strength increased with the increasing forming temperature but the elongation decreased at the same time. The square tube formed at 950 °C exhibited a highest elongation-to-failure of 15% due to the volume fraction of coarsened O phase of 19.3%. When the parts formed at 990 °C, the elongation-to-failure decreased to only 2.8%. According to these results, the O phase can act as relatively stronger phase for the microhardness at room temperature, but exhibits as ductile phase in the tensile test at 750 °C for the square tubes.

After aging treatment, the mechanical properties of the square tubes could be modified significantly, as shown in Fig. 10. Figure 10(a) displays the Vickers microhardness of square tubes aged at different temperatures. Compared to the HV 307 for the tube without aging treatment (formed at 970 °C), the microhardness was further improved. And the microhardness decreased with the increasing aging temperature, such as HV 381, HV 347 and HV 323 aged at 750, 800 and 850 °C, respectively. Both the lamellar width and volume fraction of the re-precipitated O phase contributed to this microhardness strengthening. Figure 10(b) shows the stress-strain curves tested at 750 °C. After aging treatment, the elongation-to-failure significantly increased with slight sacrificing of strength, especially for the aging temperatures of 800 and 850 °C. For example, the square tube aged at 800 °C exhibited the elongation-to-failure of 11.1% and tensile strength of 788 MPa, which were 258.1 and 87.0% of that for the square tube formed at 970 °C, respectively. O phase precipitated from the  $\beta$ /B2 phase during the aging treatment. Due to the increase in O phase content, the ductility of the alloy increased and the strength decreased at 750 °C. Grain boundary strengthening

caused by the precipitation of fine O phase increased the strength of the alloy. Therefore, the elongation of the alloy was significantly increased with slight sacrificing of strength.

The control of wall thickness and mechanical properties was the most important challenge in the forming technique of thin-wall hollow components. In order to obtain uniform thickness distribution and good comprehensive mechanical properties, the effect of forming parameters on wall thickness and the effect of heat treatment on microstructure and mechanical properties were analyzed in this paper. The forming process of components was selected as follows: forming at 970 °C and subsequent aging treatment at 800 °C for 10 h.

## 4. Conclusion

The HGPF process of Ti-22Al-24.5Nb-0.5Mo square tubes was studied by simulation and experiments at 950-990 °C. The subsequent aging treatment was performed at 750-850 °C. The results based on analysis of forming results, microstructure and mechanical properties of the formed tubes, and the effect of subsequent aging treatment on the microstructure and mechanical properties were summarized as follows:

- (1) The geometrical shape and microstructure of the formed tubes was simulated based on the uniform viscoplastic constitutive model of  $Ti_2AlNb$  based alloy. The simulation was in good agreement with the experiment results, which could guide the design of the forming process.

**Table 2 Average width and volume fraction of O phase after aging treatment**

Aging temperature	750 °C	800 °C	850 °C
Average width of O phase	90 nm	150 nm	200 nm
Volume fraction of O phase	42.8%	44.3%	45.7%

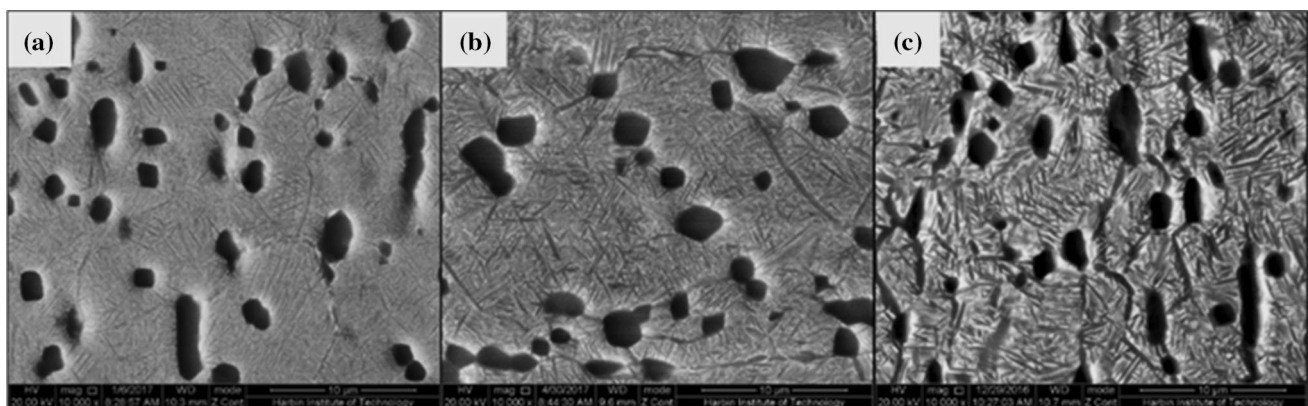


**Fig. 8** Microstructure of tubes formed at 970 °C after aging at (a) 750 °C, (b) 800 °C, (c) 850 °C

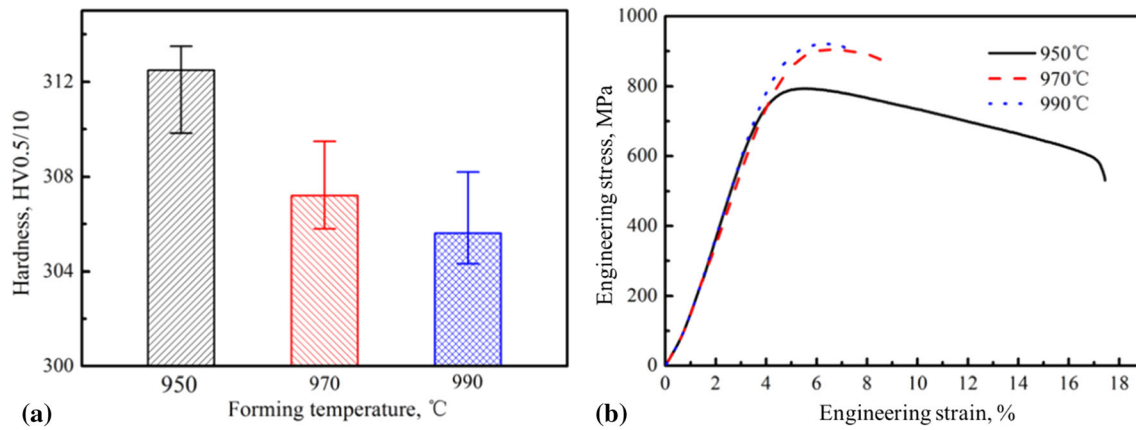


**Fig. 9** Mechanical properties for the tubes formed at different temperatures, (a) Vickers microhardness, (b) tensile curves at 750 °C

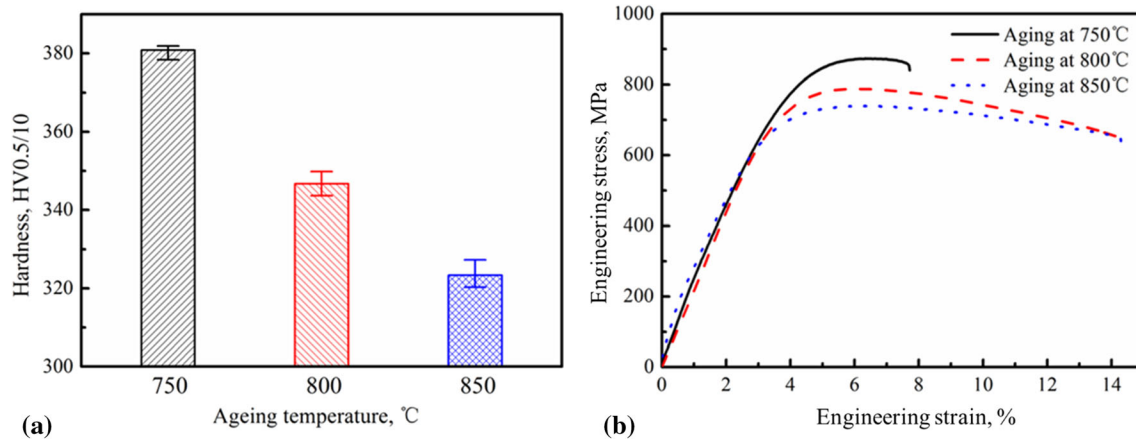


**Fig. 10** Mechanical properties for the tube aged at different temperatures, (a) Vickers microhardness, (b) tensile curves at 750 °C

- (2) Raising the forming temperature would decrease the forming time of fillet. Due to the effect of friction, the maximum thinning occurred at the transition section of the square tubes. Overall, more uniform thickness distribution can be achieved when the square tubes formed at 970 °C and 990 °C. The maximum thinning ratio was less than 19%.
- (3) The lamellar O phase dissolved during hot gas pressure forming. When the forming temperatures were above 970 °C, the O phase almost disappeared in the microstructure. And the lamellar O phase coarsened at 950 °C. At 750 °C, the tube formed at 990 °C exhibited highest peak strength of 921 MPa. When the forming temperature decreased to 950 °C, the strength decreased to 793 MPa. The elongation decreased with the increasing forming temperature. The highest elongation-to-failure was about 15% for the tubes formed at 950 °C.
- (4) After aging treatment, the elongation-to-failure at 750 °C for the square tubes formed at 970 °C was largely improved with slight sacrificing of strength. At 750 °C, the formed Ti-22Al-24.5Nb-0.5Mo square tube after aging at 800 °C exhibited comprehensively superior properties with peak strength of 788 MPa and elongation-to-failure of 11.1%. In order to obtain uniform thickness distribution and good comprehensive mechanical properties, the forming process of components was

selected as follows: forming at 970 °C and subsequent aging treatment at 800 °C for 10h.

## Acknowledgments

This work was financially supported by National High-level Personnel of Special Support Program (No. W02020239) and the National Natural Science Foundation of China (No. 51674093).

## References

1. W. Kan, Y. Liang, H. Peng, B. Chen, H. Guo and J. Lin, Microstructural Degradation of Ti-45Al-8Nb Alloy During the Fabrication Process by Electron Beam Melting, *JOM*, 2017, **69**, p 2596–2601.
2. J. Kumpfert, Intermetallic Alloys Based on Orthorhombic Titanium Aluminide, *Adv. Eng. Mater.*, 2011, **3**, p 851–864.
3. D. Banerjee, A. Gogia, T. Nandy and V. Joshi, A New Ordered Orthorhombic Phase in a Ti3Al-Nb Alloy, *Acta Metall.*, 1988, **36**, p 871–882.
4. X. Jiao, G. Liu, D. Wang and Y. Wu, Creep Behavior and Effects of Heat Treatment on Creep Resistance of Ti-22Al-24Nb-0.5Mo Alloy, *Mater. Sci. Eng. A*, 2017, **680**, p 182–189.
5. P. Lin, Y. Hao, B. Zhang, S. Zhang and J. Shen, Strain Rate Sensitivity of Ti-22Al-25Nb (at%) Alloy During High Temperature Deformation, *Mater. Sci. Eng. A*, 2018, **710**, p 336–342.

6. B. Shao, D. Shan, B. Guo and Y. Zong, Plastic Deformation Mechanism and Interaction of B2,  $\alpha 2$ , and O Phases in Ti-22Al-25Nb Alloy at Room Temperature, *Int. J. Plasticity*, 2018, **113**, p 18–34.
7. Y. Zheng, W. Zeng, D. Li, X. Liang, J. Zhang and X. Ma, Effect of Orthorhombic Case on the Creep Rupture of Ti-22Al-25Nb (at %) Orthorhombic Alloy, *Mater. Sci. Eng. A*, 2017, **696**, p 529–535.
8. A. Grigoriev, I. Polozov, V. Sufiiarov and A. Popovich, In-situ Synthesis of Ti2AlNb-Based Intermetallic Alloy by Selective Laser Melting, *J. Alloy Compd.*, 2017, **704**, p 434–442.
9. B. Shao, S. Wan, W. Xu, D. Shan, B. Guo and Y. Zong, Formation Mechanism of an  $\alpha 2$  Phase-Rich Layer on the Surface of Ti-22Al-25Nb Alloy, *Mater. Charact.*, 2018, **145**, p 205–209.
10. Z. Tan, L. Bai, B. Bai, B. Zhao, Z. Li and H. Hou, Fabrication of Lattice Truss Structures by Novel Super-plastic Forming and Diffusion Bonding Process in a Titanium Alloy, *Mater. Des.*, 2016, **92**, p 724–730.
11. C. Wang, T. Zhao, G. Wang, J. Gao and H. Fang, Superplastic Forming and Diffusion Bonding of Ti-22Al-24Nb Alloy, *J. Mater. Process. Technol.*, 2016, **222**, p 122–127.
12. W. Han, K. Zhang and G. Wang, Superplastic Forming and Diffusion Bonding for Honeycomb Structure of Ti-6Al-4V Alloy, *J. Mater. Process. Technol.*, 2007, **183**, p 450–454.
13. Z. Du, S. Jiang, K. Zhang, Z. Lu, B. Li and D. Zhang, The Structural Design and Superplastic Forming/Diffusion Bonding of Ti2AlNb Based Alloy for Four-layer Structure, *Mater. Des.*, 2016, **104**, p 242–250.
14. S. Yuan, R. Zhang and W. Zhang, Integral Hot Gas Pressure Forming of an AA2219 Aluminum Alloy Ellipsoidal Shell, *JOM*, 2017, **69**, p 742–747.
15. Y. Liu and X. Wu, A Microstructure Study on an AZ31 Magnesium Alloy Tube after Hot Metal Gas Forming Process, *J Mater. Eng. Per.*, 2007, **16**, p 354–359.
16. R. Neugebauer, T. Altan, M. Geiger, M. Kleiner and A. Sterzing, Sheet Metal Forming at Elevated Temperatures, *CIRP Ann. Manuf. Technol.*, 2006, **55**, p 793–816.
17. G. Liu, Y. Wu, D. Wang and S. Yuan, Effect of Feeding Length on Deforming Behavior of Ti-3Al-25V Tubular Components Prepared by Tube Gas Forming at Elevated Temperature, *Int. J. Adv. Manuf. Tech.*, 2015, **81**, p 1809–1816.
18. K. Wang, G. Liu, J. Zhao, J. Wang and S. Yuan, Formability and Microstructure Evolution for Hot Gas Forming of Laser-Welded TA15 Titanium Alloy Tubes, *Mater. Des.*, 2016, **91**, p 269.
19. C. Boehlert, The Phase Evolution and Microstructural Stability of an Orthorhombic Ti-23Al-27Nb Alloy, *J. Phase. Equilib.*, 1999, **20**(2), p 101.
20. Y. Wu, D. Wang, Z. Liu and G. Liu, A Unified Internal State Variable Material Model for Ti2AlNb-Alloy and its Applications in Hot Gas Forming, *Int. J. Mech. Sci.*, 2019, **164**, p 105126.
21. G. Liu, S. Yuan and B. Teng, Analysis of Thinning at the Transition Corner in Tube Hydroforming, *J. Mater. Process. Tech.*, 2006, **177**, p 688–691.
22. W. Wang, W. Zeng, C. Xue, X. Liang and J. Zhang, Quantitative Analysis of the Effect of Heat Treatment on Microstructural Evolution and Microhardness of an Isothermally forged Ti-22Al-5Nb (at.%) Orthorhombic Alloy, *Intermetallics*, 2014, **45**, p 29–37.
23. C. Xue, W. Zeng, W. Wang, X. Liang and J. Zhang, Coarsening Behavior of Lamellar Orthorhombic Phase and its Effect on Tensile Properties for the Ti-22Al-25Nb Alloy, *Mater. Sci. Eng. A*, 2014, **611**, p 320–325.
24. C. Boehlert, B. Majumdar, V. Seetharaman and D. Miracle, Part I. The Microstructural Evolution in Ti-Al-Nb O+Bcc Orthorhombic Alloys, *Metall. Mater. Trans. A.*, 1999, **30**, p 2305–2323.
25. A. Gogia, T. Nandy, D. Banerjee, T. Carisey, J. Strudel and J. Franchet, Microstructure and Mechanical Properties of Orthorhombic Alloys in the Ti-Al-Nb System, *Intermetallics*, 1998, **6**, p 741–748.
26. C.J. Boehlert, Part III. The tensile behavior of Ti-Al-Nb O+Bcc Orthorhombic alloys, *Metall. Mater. Trans. A.*, 2001, **32**, p 1977–1988.

**Publisher's Note** Springer Nature remains neutral with regard to jurisdictional claims in published maps and institutional affiliations.